Proceedings of ICONE14
International Conference on Nuclear Engineering
July 17-20, Miami, Florida, USA

ICONE14-89608

APPLICATION OF NEAR WALL MODEL TO LARGE EDDY SIMULATION BASED ON BOUNDARY LAYER APPROXIMATION

Takashi TAKATA
Graduate School of Engineering, Osaka University
2-1, Yamada, Suita, Osaka, 565-0871, Japan
Phone: +81-6-6879-7895 Fax: +81-6-6879-7889
Email : takata_t@nucl.eng.osaka-u.ac.jp

Akira YAMAGUCHI
Graduate School of Engineering, Osaka University
2-1, Yamada, Suita, Osaka, 565-0871, Japan
Phone: +81-6-6879-7890 Fax: +81-6-6879-7889
Email : yamaguchi@nucl.eng.osaka-u.ac.jp

Masaaki TANAKA
Japan Atomic Energy Agency
4002, Narita, O-arai, Ibaraki, 311-1393, Japan
Phone: +81-29-267-4141 Fax: +81-29-267-3675
Email: tanaka.masaaki@jaea.go.jp

Hiroyuki OHSHIMA
Japan Atomic Energy Agency
4002, Narita, O-arai, Ibaraki, 311-1393, Japan
Phone: +81-29-267-4141 Fax: +81-29-267-3675
Email: ohshima.hiroyuki@jaea.go.jp

ABSTRACT

Turbulent statistics near a structural surface, such as a magnitude of temperature fluctuation and its frequency characteristic, play an important role in damage progression due to thermal stress. A Large Eddy Simulation (LES) has an advantage to obtain the turbulent statistics especially in terms of the frequency characteristic. However, it still needs a great number of computational cells near a wall.

In the present paper, a two-layer approach based on boundary layer approximation is extended to an energy equation so that a low computational cost is achieved even in a large-scale LES analysis to obtain the near wall turbulent statistics.

The numerical examinations are carried out based on a plane channel flow with constant heat generation. The friction Reynolds numbers (Re_τ) of 395 and 10,000 are investigated, while the Prandtl number (Pr) is set to 0.71 in each analysis.

It is demonstrated that the present method is cost-effective for a large-scale LES analysis.

NOMENCLATURE

Cp	specific heat
Cs	Smagorinsky constant
$\mathbf{g}$	gravity vector
h_e	enthalpy
p	kinetic pressure
Pr_t	turbulent Prandtl number
Q	heat generation per unit volume
q_w	heat flux at wall
Re (=$2hU/\nu$)	Reynolds number based on average velocity (U) and channel height ($2h$)
Re_τ (=$h\,u_\tau/\nu$)	friction Reynolds number
$\|\mathbf{S}\|$	magnitude of total strain tensor
T	temperature
T^+ (=$(T_w-T)/T_\tau$)	dimensionless temperature
T_τ (=$q_w/(\rho Cpu_\tau)$)	friction temperature
t	time
t^* (=tu_τ/h)	dimensionless time
$\mathbf{u}$	velocity vector
u_τ	friction velocity
x_k	coordinate in normal direction against wall
y^+ (=$u_\tau y/\nu$)	dimensionless height
α	smoothing factor
κ	Kármán constant
λ	thermal conductivity
μ	molecular viscosity
ν	kinetic viscosity
ν_{SGS}	eddy (SGS) viscosity in outer layer
ν_t	eddy viscosity in inner layer
ρ	density

ρ_o	reference density
τ_w	wall shear stress
$\bar{}$	spatial filtering

INTRODUCTION

In a nuclear power plant, a structural integrity caused by turbulent fluid dynamics is of great concern. For instance, a thermal striping phenomenon will occur downstream a flow junction of different temperatures and a piping system may be influenced due to thermal stress. In the thermal striping phenomenon, frequency characteristics of fluid temperature fluctuation near the piping wall surface play an important role in damage progression, as well as a magnitude of the fluctuation (Kasahara, 1999).

A Large Eddy Simulation (LES) has an advantage to obtain turbulent statistics, such as a magnitude of fluctuation and its frequency characteristics, compared with the Reynolds Average Navier-Stokes (RANS) model. And it can save computational resources rather than the Direct Numerical Simulation (DNS).

However, LES method still requires a great number of computational nodes especially near a wall, when one applies it to large scale engineering problems such as a high-Reynolds number situation (Piomelli, 2002). Consequently, the effect of wall layer will be taken into account separately using such as the wall function (Morinishi, 1989), the equilibrium laws (Deardorff, 1970) and the boundary layer approximation (Balaras, 1996) to overcome this problem for a large scale analysis, which are well known as the Two-Layer Model (TLM).

The boundary layer approximation has major two advantages compared with the other TLM approaches. Since separate grids are implemented near wall in the boundary layer approximation, the thermal-hydraulic information near the wall, such as a velocity, temperature and fluctuations of them, can be evaluated easily. Especially, the temperature information near the wall is quite important as mentioned above. The other is that this model can be applicable in any complicated fluid configuration. Typically, the wall function has less accuracy in a natural convection configuration because it is determined based on forced convection configurations.

In the present paper, a simplified boundary layer approximation, originally proposed by Balaras (1996), is extended to an energy equation so that a low computational cost is achieved even in a large scale LES analysis to obtain near wall turbulent statistics. Numerical examinations of the present method are carried out using a plane channel turbulence with constant heat generation in condition of Re_τ = 395 and 10,000. In case of Re_τ = 395, the numerical results and the computational cost of the present method are compared with that of DNS, LES with near wall resolution (LES-NWR) and the wall function approximation. The capability of the present method is also investigated in the high Reynolds number condition of Re_τ = 10,000.

LES WITH BOUNDARY LAYER APPROXIMATION

In the boundary approximation, a separated series of mesh is embedded on a wall boundary as an inner layer. Figure 1 shows the schematic of the mesh arrangement.

In the inner layer, velocity and temperature are solved using boundary layer equations referring to the adjacent outer layer variables. At the same time, the inner layer region is also taken into consideration as an average in the coarse LES of outer layer. The interaction between the coarse LES and the wall, such as a shear stress and a heat flux, is estimated from a direct differential in the inner layer resolution. When the inner layer equations are solved as a kind of simple LES or unsteady RANS method, it is conceivable that turbulent statistics will be obtained cost-effectively.

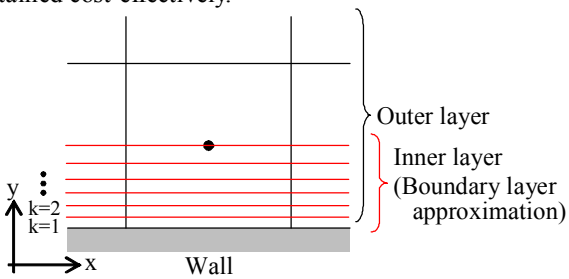

Fig.1 Inner layer mesh arrangement

In the following section, governing equations, numerical procedure and coupling manner are described.

Governing equations

With regard to a velocity, the following governing equations of mass and momentum are considered.

[Mass]

$$\frac{\partial \bar{\rho}}{\partial t} + \nabla \cdot \bar{\rho}\bar{\mathbf{u}} = 0 \tag{1}$$

[Momentum]

$$\bar{\rho}\frac{\partial \bar{\mathbf{u}}}{\partial t} + \nabla \cdot \bar{\rho}\bar{\mathbf{u}}\bar{\mathbf{u}} = -\nabla \bar{p} + \frac{\partial}{\partial x_k}\left[(\bar{\mu} + \bar{\rho}\nu_t)\frac{\partial \bar{\mathbf{u}}}{\partial x_k} \right] + (\bar{\rho} - \rho_0)\mathbf{g} \tag{2}$$

As shown in Eqs. (1) and (2), each variable in an inner cell is treated as a spatial filtered one which is same as a general LES method.

In general use of boundary approximation, the following two terms are ignored; the convection term ($\nabla \cdot \bar{\rho}\bar{\mathbf{u}}\bar{\mathbf{u}}$) in the normal-wise direction vertically to a wall and the diffusive term (second term at the right hand side in Eq. (2)) both in the stream- and span-wise directions. In the present method, the convection term in all directions is taken into account to investigate Grid-Scale turbulence in the inner layer. On the contrary, the same assumption is adopted in the diffusive term. It is attributed the fact that the stream- and span-wise diffusive

term is negligible compared with that in the normal-wise direction because of a large aspect of mesh arrangement embedded in the inner layer.

The determination of the eddy viscosity (ν_t) is of great concern in the present method. Balaras (1996) proposed the simple model based on the mixing length theory in the boundary layer approximation. In the present paper, the similar eddy viscosity is considered for simplicity as;

$$\nu_t = \alpha(\kappa y)^2 D|\mathbf{S}| \tag{3}$$

Here, κ is Karman's constant. In the present paper, κ is set to 0.4 and the smoothing factor (α in Eq. (3)) is multiplied so as to moderate the eddy viscosity and to obtain the continuous distribution between the inner and outer layers. D is Van Driest type damping factor. α and D are defined in the following.

$$\alpha = \left.\frac{\nu_{SGS}}{(\kappa y)^2 D\,|\,\mathbf{S}\,|}\right|_{\text{upper end boundary}} \tag{4}$$

$$D = 1 - \exp[-(y^+/25)^3] \tag{5}$$

In addition to governing equations of mass and momentum, the following energy equation is made consideration in the present paper.

[Energy]

$$\overline{\rho}\overline{Cp}\frac{\partial \overline{T}}{\partial t} + \nabla\cdot\overline{\rho}\overline{h}_e\overline{\mathbf{u}} = \frac{\partial}{\partial x_k}\left[(\overline{\lambda} + \frac{\overline{\rho}\overline{Cp}\nu_t}{Pr_t})\frac{\partial \overline{T}}{\partial x_k}\right] + Q \tag{6}$$

The convection and diffusive terms in Eq. (6) are treated as in the momentum equation. It is noted that both the temperature and the enthalpy are used as an induced variable in order to estimate the convection term with accuracy.

Discretization and numerical procedure

For the purpose of reducing computational cost, the pressure gradient (∇p) in Eq. (2) is considered as a source term and is calculated based on that in the outer layer (coarse LES) adjacent to the inner layer (originally proposed by Balaras, 1996). Hence, one does not need to solve the Poisson equation for pressure in the inner layer. Taking Top-Hat filter into account, a second order central differential scheme is applied both in the convection and diffusive terms. The convection term is calculated explicitly, whereas an implicit manner is adopted in the diffusive term to avoid a numerical instability. As concerns the time dependant term, the second order three-point implicit scheme is applied.

As a result of discretization in Eq. (2), it is re-written as,

$$a_k u_k = b_{k-1}u_{k-1} + b_{k+1}u_{k+1} + d_k \tag{7}$$

Here, a, b and d are constant and are calculated explicitly in each time step. The reduction technique of u_{k+1} from Eq. (7) is used to avoid an iterative solution.

Since the pressure gradient is a priori estimated, it is not necessarily the case that the mass balance is fulfilled when one solves the momentum equations in all directions. Therefore, the stream- and span-wise velocities are estimated from Eq. (2), while the velocity in the normal-wise direction is calculated based on the updated stream- and span-wise velocity and mass balance (Eq. (1)). In terms of the energy equation, exact the same discretization with the momentum equation is applied.

The numerical procedure in the inner layer is described in the following. First of all, the temperature field is updated using Eq. (6) and the density in each cell is renewed based on the updated temperature and the equation of state. The next step is to estimate the stream- and span-wise velocity field in each column of the layer (Eq. (2)). Then, the normal-wise velocity profile is obtained by Eq. (1).

With regard to the outer layer computation (LES), a finite differential scheme of the SMAC method with a second order (central differential in convection and diffusive terms, Adams-Bashforth in time marching) is applied using a structural mesh arrangement in the present paper. The usage of a simple second order scheme allows for an engineering application of LES. Both in the inner and outer layer, a staggered grid is implemented for velocity field.

Coupling manner

From the outer layer, the velocity and the temperature are released to the inner layer as a boundary value at the upper end which is allocated at the center of the adjacent outer layer (Fig. 1). As concerns the pressure gradient, the same value of the outer layer is added as a source term through the column of the inner layer.

A finite difference is used simply at a bottom cell of inner layer adjacent to a wall to obtain the shear stress ($\boldsymbol{\tau}_w$) and the heat flux (q_w) on the wall surface, which are required in the outer layer computation.

$$\boldsymbol{\tau}_w = \eta_{k=1}\frac{\mathbf{u}_{k=1} - 0}{1/2\Delta y_{k=1}},\quad q_w = \lambda_{k=1}\frac{T_w - T_{k=1}}{1/2\Delta y_{k=1}} \tag{8}$$

It is noted that no turbulent effect is taken into account between the bottom cell of inner layer and the wall as seen in Eq. (8).

In addition, the stream- and span-wise velocity gradients at the cell center of the outer layer adjacent the inner layer, which are referred in the rate of strain tensor to estimate the Sub-Grid Scale eddy viscosity, are also calculated based on the velocities at the upper end of the inner layer and at the center of the adjacent outer layer.

PLANE CHANNEL FLOW ANALYSES

The applicability of the present method is examined numerically with a wall turbulence configuration. A plane channel flow with constant heat generation is selected for this purpose. The analytical geometry is shown in Fig. 2.

The size of analytical region is $2\pi(x)\times2(y)\times\pi(z)$ [m] and the periodical condition is applied both in the stream- and span-wise directions. The constant pressure gradient calculated theoretically by the friction Reynolds number (Re_τ) is added as

a driving force in the momentum equation. In the present paper, analyses of Re_τ = 395 and 10,000 are carried out. These correspond to approximately 14,000 and 542,000 of the Reynolds number based on the mean stream-wise velocity and the channel height respectively. In case of Re_τ=395, three models are examined; the near wall resolution (NWR), the wall function (WF) and the boundary layer approximation (BLA), whereas the WF and the BLA cases are tested in the higher Reynolds number condition (Re_τ=10,000). In the WF case, the Spaulding function (Spaulding, 1961) and the Kader's equation (Kader, 1981) are used as a wall function for velocity and temperature respectively.

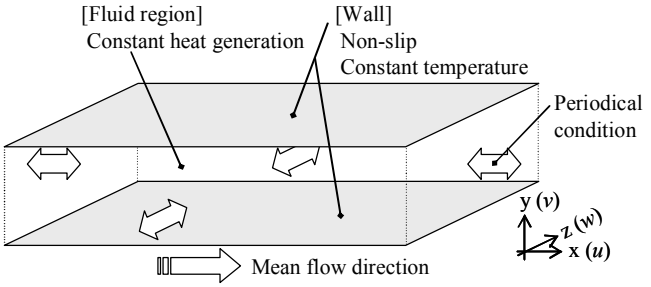

Fig. 2 Analytical geometry

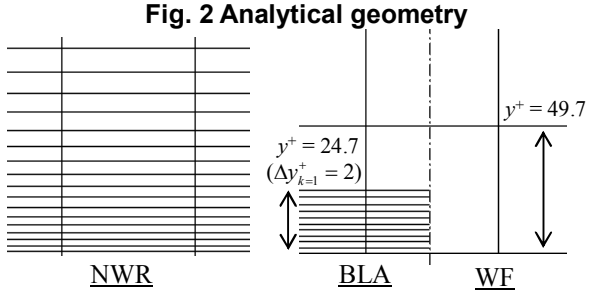

(a) Re_τ = 395

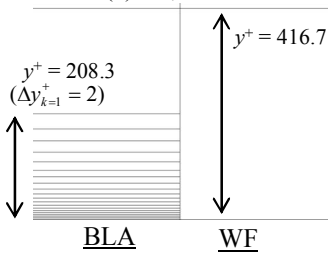

(b) Re_τ = 10,000

Fig. 3 Mesh arrangement near wall boundary

Both in case of Re_τ=395 and 10,000, a uniform structural mesh divided into 48 cells is embedded in the stream- and the span-wise directions. On the other hand, the mesh arrangement in the normal-wise direction differs with the Reynolds number and the model. Fig. 3(a) shows the mesh arrangements near the wall in case of Re_τ=395. An irregular series of 64 meshes, which increases geometrically from the wall to the channel center, is implemented in the NWR case. In the WF case and the outer layer of the BLA, a uniform mesh divided into 16 cells is embedded. With regard to the inner layer of the BLA, the analytical region is divided into an irregular series of 10 meshes. In case of Re_τ=10,000, 48 meshes uniform in size are applied both in the WF and BLA cases. In the inner layer of the BLA, 20 meshes of a geometric progression are implemented as shown in Fig. 3(b).

It is noted that the geometric progressions in the NWR and the inner layer of the BLA are arranged so that the half height at the first cell adjacent to the wall ($\Delta y^+/2$) becomes approximately unit.

As concerns the temperature analysis, a constant heat generation through the computational region and a constant temperature at wall boundary are assumed (see Fig. 2). The Prandtl number and the turbulent Prandtl number are set to 0.71 and 0.85 respectively. In the present analyses, the temperature is treated as a passive scalar and thus the buoyancy effect is ignored.

In the LES computation, the standard Smagorinsky model (Cs=0.1) is applied as the SGS eddy viscosity. In addition, the SGS eddy viscosity is multiplied by the Van Driest type damping factor in the NWR case.

Table 1 summaries the analytical condition. In each computation, the Grid-Scale (GS) data is accumulated during approximately 20 of the dimensionless time (t^*) after the turbulent state is fully developed. In the following figures, the results are arranged using the GS data.

Table 1 Analytical conditions

[Geometry and mesh arrangement]		
	Size :	2π(x)×2(y)×π(z) [m]
	Mesh arrangement:	
	(stream- and span-wise)	
		48(x) ×48(z)
	(normal-wise)	
· Reτ=395		
	NWR	64(y) (stretching factor 1.10)
	WF	16(y) (uniform)
	BLA	16(y) (uniform, outer layer)
		10(y) (stretching factor 1.04,
· Reτ=10,000		inner layer)
	WF	48(y) (uniform)
	BLA	48(y) (uniform, outer layer)
		20(y) (stretching factor 1.15,
[SGS model in LES]		inner layer)
	NWR:	Standard Smagorinsky (Cs=0.1) with Van Driest type damping factor
	WF, BLA:	Standard Smagorinsky (Cs=0.1)
[Friction Reynolds number]		
	Re_τ:	395 and 10,000
[Prandtl number]		
	Pr:	0.71
	Pr_t:	0.85

Reτ=395

Figure 4 shows the mean profiles of the stream-wise velocity and the temperature perpendicular to the wall. The dashed line indicates the empirical wall functions. The DNS result (Kawamura, 1998) is also shown with the solid line in Fig. 4. In each analysis, the mean profiles perpendicular to the

wall agree relatively with that of the empirical law and/or the DNS data. In case of the NWR, the mean velocity and the mean temperature near the center are slightly underestimated compared with the DNS data. It will be attributed the fact that the spatial resolution is not sufficient in the present analysis.

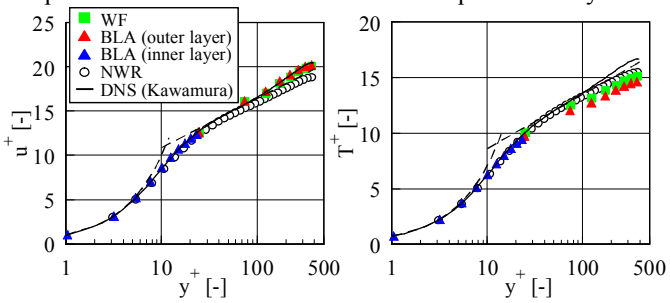

Fig. 4 Mean profiles (Re_τ=395)

In the WF and the outer layer of the BLA, the spatial resolution is coarser than that in the NWR. Furthermore, a near wall approximation is adopted in each case. Accordingly, inaccuracy should be enlarged in the WF and BLA cases. As shown in the left side of Fig. 4, the results in the WF and BLA cases seem to be better than that in the NWR case in terms of the mean velocity. However, it will not be demonstrated that the higher predictive accuracy is obtained by the WF and the BLA models.

With regard to the inner layer of the BLA, it is demonstrated that the good agreement with the DNS and the NWR data is obtained as shown in Fig. 4.

The distributions of the velocity and temperature fluctuation are shown in Fig. 5. In the left side of Fig. 5, the fluctuation through the channel center (y^+<400) is indicated, whereas the distribution is closed up (y^+<50) in order to reveal the near wall information in the right side of Fig. 5. The distributions of the fluctuation in the outer layer of the BLA have almost no difference from that in the WF case and agree with that of the DNS and the NWR results.

As seen in the Fig. 5(a) and (d), the stream-wise velocity and the temperature has a maximum in case of the DNS and the NWR at y^+≈15, which is allocated in the inner layer of the BLA. In the present method (BLA), the values of the outer layer cell adjacent to the wall are almost the same with those of the WF and are underestimated compared with the DNS and the NWR (see the red and green rectangles in the right side of Fig. 5). However, in the inner layer of the BLA, the fluctuation intensity increases gradually from the upper end boundary toward the wall and approximates to that of the DNS and the NWR. Since the peak depends strongly upon a flow structure very near the wall, it might be said that the flow pattern very near the wall is reconstructed in the present method although an outer layer value that is already filtered spatially using a coarse mesh is assigned as a boundary.

As shown in Fig. 5(b) and (c), when the boundary values between the inner and outer layers agree with that of the DNS or the NWR, it is demonstrated that the distribution is re-simulated well with the present method.

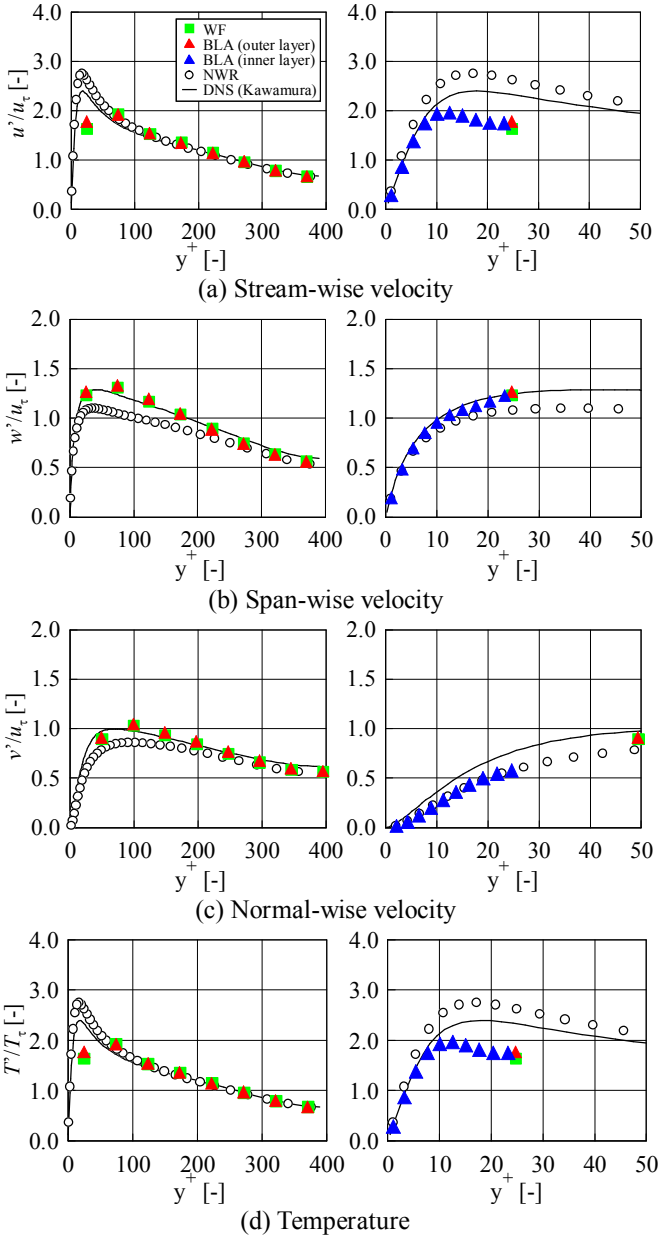

Fig. 5 Magnitude of fluctuation (Re_τ=395)

Let us discuss the frequency characteristic of the temperature. Figure 6 shows the Auto-Power Spectral Density (APSD) of the dimensionless temperature (T^+) at the channel center (y^+≈400, solid lines) and the very near wall (y^+≈5, dashed lines). In Fig. 6, the sampling frequency and the duration are set to 500Hz and 5sec respectively.

At the channel center, almost the similar frequency characteristic is investigated regardless of the models below approximately 20Hz. Oh the other hand, the power density of the BLA is comparatively higher than the others and coincides with that near the wall at the high range of frequency (>20Hz).

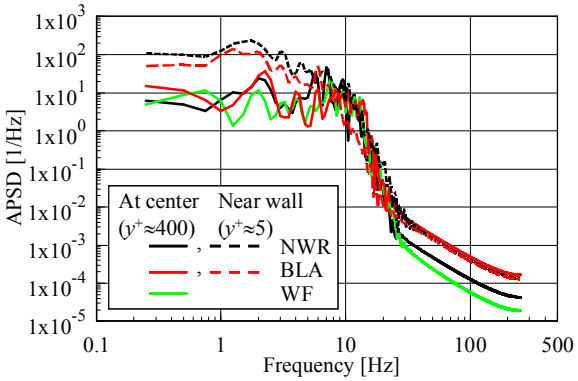

Fig. 6 Auto-Power Spectral Density of dimensionless temperature (Re_τ=395)

When it comes to the wall, the peak frequency seems to shift to a lower range both in the NWR and the BLA cases. Comparing the frequency characteristic with the NWR case, almost the same but a little bit weakened profile is investigated in the inner layer of the BLA. It is noted that no information near the wall can be obtained from the WF case.

In the near wall region, the power density at high frequency will increase due to an enhancement of the GS resolution. In the NWR case, the high frequency mode of the power density investigated near the wall is weakened through the channel center, while a little damping is predicted in the BLA case. Possibly, the discontinuous change of the mesh connection at the boundary between the inner and the outer layers affects the damping at the high frequency.

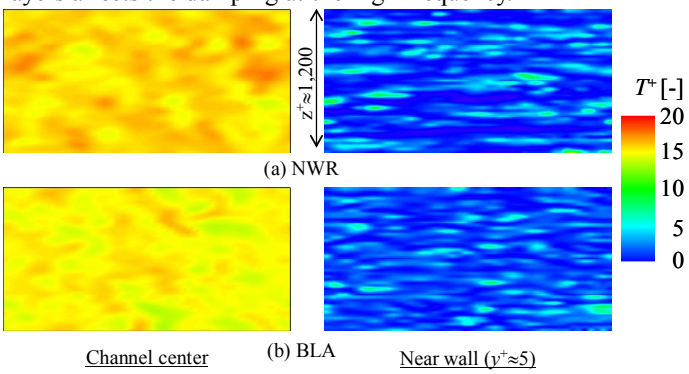

Fig. 7 Instantaneous temperature distribution (Re_τ=395)

The shift of the peak frequency will be explained with the fact that the flow structure near the wall differs from that at the channel center. The instantaneous distribution of the dimensionless temperature horizontally to the wall is shown in Fig. 7. As shown in Fig. 7(a), no obvious regular flow structure is predicted at the channel center, while a streak structure is investigated near the wall. The span of the streak is $z^+\approx100$, which corresponds to that observed in the experiments and the DNS analysis. Consequently, the regular structure of the streak causes the peak frequency to shift to a lower range. As seen in Fig. 7(b), similar pattern is confirmed in the inner layer of the BLA. It may be concluded that the flow structure near wall will be re-constructed in a moderate wall turbulence of Re_τ=395 using the present method.

Table 2 Computational cost (Re_τ=395)

	NWR	BLA	WF
Mesh (cells)	48×64×48 (147,500)	48×36*×48 (82,900)	48×16×48 (36,900)
Cost	**3.84**	**1.21**	**1.00**

*including cells in inner layer

The computational cost, which is normalized by the result of the WF case, is summarized in Table 2. The present method (BLA) requires only 20% of increase compared with the WF so as to obtain the near wall turbulent information that agrees relatively with the DNS data and the NWR. It is demonstrated that the present method is quite cost-effective.

Reτ=10,000

Figure 8 shows the mean profiles of the stream-wise velocity and the temperature perpendicular to the wall. Since there is no DNS data in such a high friction Reynolds number, only the empirical functions are drawn with the dashed line in Fig. 8.

In the WF case, the mean profiles of the velocity and the temperature is close to that of the empirical functions. When the wall function is applied to a first grid adjacent to a wall, the values at the first grid are forced into following the function. At the second grid from the wall ($y^+\approx600$ in the present analysis) and above, the influence of the wall becomes small and thus a comparative large scale of turbulence will be dominant. Therefore, almost the similar profiles with the wall functions are obtained regardless of the coarse mesh arrangement.

In case of the BLA, although the mean velocity is overestimated slightly by approximately 10%, the mean profiles agree with the empirical functions including the inner layer region. It is noted that the determination of the eddy viscosity in the inner layer is of great importance. The influence of the eddy viscosity on the turbulent phenomena in the inner layer will be future work.

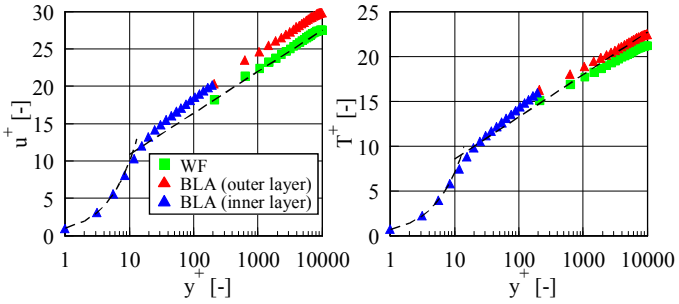

Fig. 8 Mean profiles (Re_τ=10,000)

Figure 9 shows the distributions of the fluctuation. It is demonstrated that there is almost no difference in terms of the

fluctuation profiles between the WF and the outer layer of BLA cases, as well as in case of Re_τ=395. As shown in the left side of Fig. 9(a), the peak of the fluctuation appears clearly at the second grid of the outer layer (y^+≈600) from the wall in the stream-wise velocity. This might be attributed the fact that the SGS viscosity increases rapidly at the first grid point due to high gradient of the stream-wise velocity along the normal-wise direction, resulting in the increase of the kinetic energy in the SGS at that point. Consequently, the kinetic energy evaluated in the GS is diluted in total.

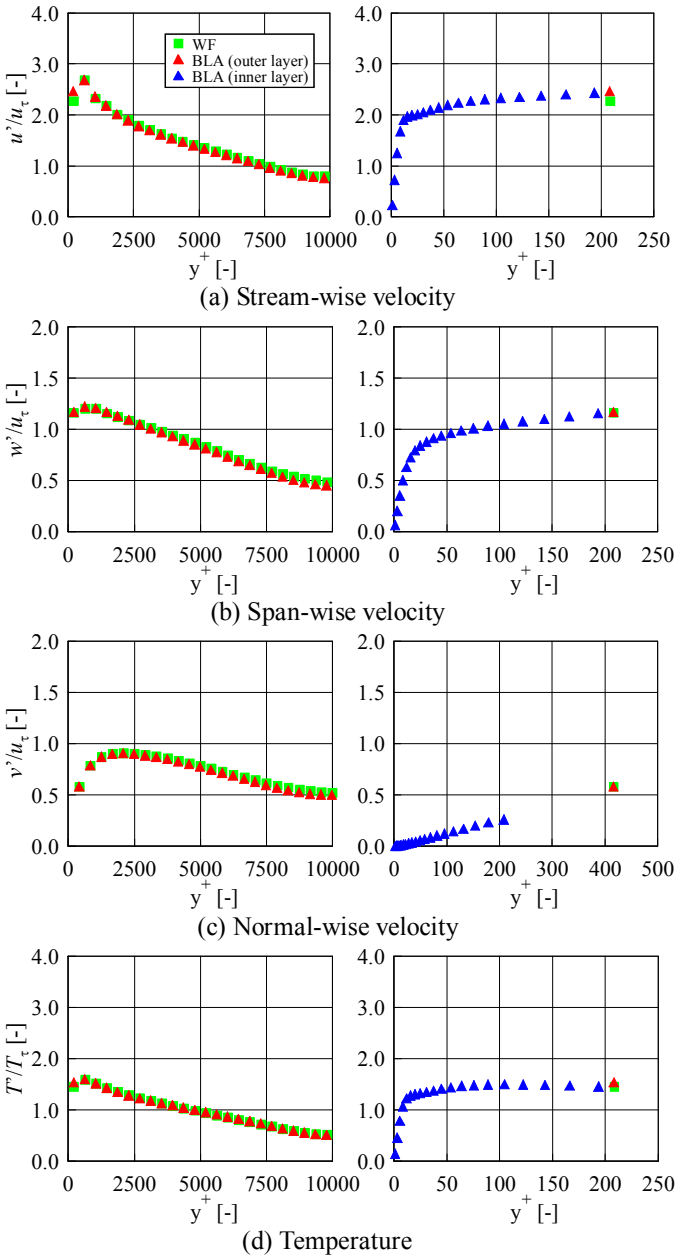

Fig. 9 Magnitude of fluctuation (Re_τ=10,000)

In the inner layer of the BLA, the magnitude of the fluctuation decreases gradually from the upper end boundary except the normal-wise velocity fluctuation. Then it suddenly decreases at y^+≈10-20 as seen in case of Re_τ=395. However, the fluctuation intensity peak of the stream-wise velocity and the temperature disappears in case of Re_τ=10,000. As concerns the normal-wise root-mean-square, it decreases proportionately, since it already tends to decrease near the wall in the outer layer. Probably, the streak structure can not be re-constructed in Re_τ=10,000 condition, resulting in the no peak in the inner layer (discussed later).

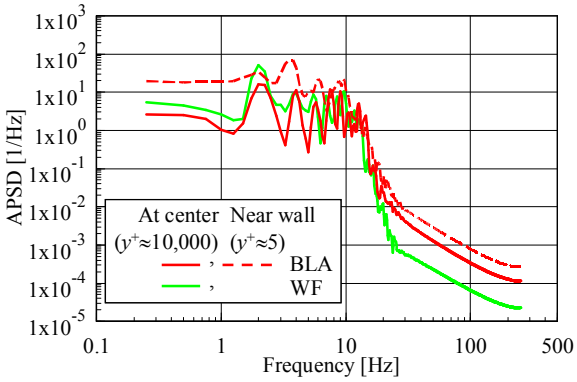

Fig. 10 Auto-Power Spectral Density of dimensionless temperature (Re_τ=10,000)

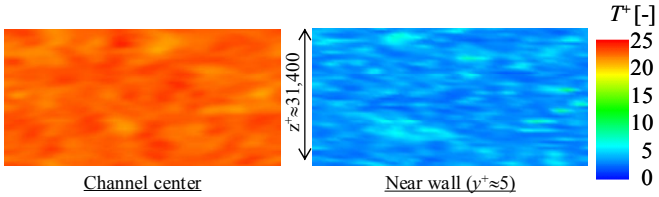

Fig. 11 Instantaneous temperature distribution in BLA (Re_τ=10,000)

The frequency characteristics of the dimensionless temperature at the center and near the wall are shown in Fig. 10. At the center, the frequency characteristic seems to be close between the WF and the BLA cases except the high frequency range of over 20Hz, as well as in case of Re_τ=395. The peak of the frequency seems to move to a lower range toward the wall boundary. However, the shift is obfuscated rather than that in Re_τ=395 condition.

Figure 11 shows the instantaneous fields of the dimensionless temperature horizontally to the wall in Re_τ=10,000. As shown in the right side of Fig. 11, no streak structure is investigated. In case of Re_τ=10,000, the dimensionless distance of the span-wise direction in the analysis region (z^+) is approximately 31,400 and the uniform mesh arrangement divided into 48 segments is implemented. It is obvious that the present analysis has not sufficient spatial resolution to re-simulate the streak structure, which will appears at z^+≈100 intervals. Consequently, no fluctuation peak will be investigated in the present method. However, it is also the fact that one may not require such a high resolution, for instance, in a thermal striping phenomenon of a reactor piping

system. More examination will be carried out with regard to the predictive reliability of the present method.

The computational cost in case of Re_τ=10,000 is revealed in Table 3. Only an increase by 10% requires so as to estimate the turbulent information compared with the WF case. It is demonstrated again that the present method is quite cost-effective.

Table 3 Computational cost (Re_τ=10,000)

	BLA	WF
Mesh (cells)	48×88*×48 (202,800)	48×48×48 (110,600)
Cost	**1.11**	**1.00**

*including cells in inner layer

CONCLUSIONS

The boundary layer approximation approach near the wall is applied to the Large Eddy Simulation both in a velocity and a temperature fields so that one can obtain the turbulent statistics, such as a magnitude of fluctuation and a frequency characteristic of the fluctuation in terms of a velocity and a temperature, with a little increase of computational cost. The applicability and capability is investigated numerically in a wall turbulence of plane channel flow with a constant heat generation.

When the present method is examined in a moderate turbulence of Re_τ=395, it is demonstrated that almost similar results with the DNS and the Near Wall Resolution LES are predictive with regard to the variation profile and its frequency characteristics of the velocity and the temperature. It is concluded that the turbulent structure of velocity and temperature near the wall will be re-constructed using the present method.

In case of Re_τ=10,000, the average profiles of the velocity and the temperature agree with that in an empirical wall function. As concerns the turbulent statistics near the wall, it is demonstrated that the sudden decrease of the fluctuation at $y^+\approx$10-20 is investigated as well as in case of Re_τ=395. However, the fluctuation intensity peaks that will appear at $y^+\approx$20 are not predicted in terms of the stream-wise velocity and the temperature fluctuations. This might be attributed the fact that the Grid-Scale resolution is not sufficient in the present analysis to reveal a microscopic structure due to turbulence with a high Reynolds number. In the future work, the predictive reliability of the near wall turbulent statistics will be examined more especially in a high Reynolds number configuration.

With regard to the computational cost of the present method, it is demonstrated that only an increase by 10-20% is required compared with the LES using the wall function so as to estimate the near wall turbulent information. It is obvious that the present method is quite cost-effective and is useful for a large scale LES analysis.

REFERENCES

Balaras E., et al., 1996, "Two-Layer Approximate Boundary Conditions for Large-Eddy Simulations", *AIAA Journal, Vol.34, No. 6*, pp.1111-1119

Deardorff JW., 1970, "A Numerical Study of Three-Dimensional Turbulent Channel Flow at Large Reynolds Numbers ", *J. Fluid Mech. Vol. 41*, pp.453-480

Kasahara N., 1999, "Evaluation of Thermal Striping Phenomena at a Tee Junction of LMFR Piping System with Numerical Methods (2) Thermomechanical Calculations", *Proc. of 15th Structural Mechanics in Reactor Technology (SMiRT)*, Seoul, Korea, F05/5

Karder B. A., 1981, "Temperature and Concentration Profiles in Fully Turbulent Boundary Layers", *Int. J. Heat Mass Transfer, Vol. 23, No. 9*, pp.1541-1544

Kawamura H, et al., "DNS of Turbulent Heat Transfer in Channel Flow with Respect to Reynolds-Number Effect", *2nd EF Conference Turbulent Heat Transfer, Manchester, Vol. 1*, pp. 1.15-1.22

Morinishi Y. and Kobayashi T., 1989, "A Study on Wall Boundary Condition in LES", *Trans. Of the JSME B, Vol. 55, No. 511*, pp.615-623 [in Japanese]

Piomelli U. and Balaras E., 2002, "Wall-Layer Models for Large-Eddy Simulation", *Annu. Rev. Fluid Mech. Vol. 34*, pp.349-374

Spaulding, D. B., 1961, "A Single Formula for the Low of the Wall", *Trans. ASME, J. Appl. Mech, Vol. 28*, pp.455-458